JMEPEG (2004) 13:316-326
DOI: 10.1361/10599490419306

1059-9495/$19.00

Rupture Testing as a Tool for Developing Planar Solid Oxide Fuel Cell Seals

K. Scott Weil, John E. Deibler, John S. Hardy, Dong Sang Kim, Guan-Guang Xia, L.A. Chick, and Chris A. Coyle

(Submitted 5 January 2004)

One of the critical issues in designing and fabricating high-performance planar solid oxide fuel cell (pSOFC) stacks is the ability to hermetically seal adjacent metal and ceramic components. In our pSOFC development program, we have designed a testing technique that allows us to screen through the numerous variables involved in developing glass seals. Using this test for example, we have found that the composition of the metal component plays an important role in the strength of the seal. Microstructural analysis of as-sealed specimens revealed that an interfacial reaction zone forms during joining, and it appears that the thickness and composition of this layer are the dominant parameters that control joint strength. In this paper the details of the seal test are reported. The results have proven particularly significant in the development of the next-generation stack design. Supporting microstructural and chemical analyses collected on the test specimens are also presented and used to interpret the seal test results in an effort to identify the necessary steps toward improving glass pSOFC seals.

Keywords glass seal, rupture strength testing, solid oxide fuel cell (SOFC), thermal cycling

1. Introduction

Solid oxide fuel cells function due to an oxygen ion gradient that develops across the yttria-stabilized zirconia (YSZ) electrolyte membrane via ionic transport when one side is exposed to an oxygen-rich environment, such as air, and the other side to a reducing gas. To maintain this gradient, and thereby maximize the performance of the device, the electrolyte and the joint that seals this membrane to the device chassis must be hermetic. That is, the YSZ layer must be dense, must not contain interconnected porosity, and must be connected to the rest of the device structure with a high temperature, gas-tight seal. With planar SOFCs, recent advances in the tape casting of thin, anode-supported ceramic bilayers have successfully addressed the first two issues.[1] The remaining challenge is to develop a consistent method of joining the ~10 μm thick electrochemically active YSZ electrolyte to the metallic structural component such that the resulting seal is hermetic, rugged, and stable under both thermal cycling and continuous long-term high-temperature operation.

This paper was presented at the Fuel Cells: Materials, Processing, and Manufacturing Technologies Symposium sponsored by the Energy/Utilities Industrial Sector & Ground Transportation Industrial Sector and the Specialty Materials Critical Technologies Sector at the ASM International Materials Solutions Conference, October 13-15, 2003, in Pittsburgh, PA. The symposium was organized by P. Singh, Pacific Northwest National Laboratory, S.C. Deevi, Philip Morris USA, T. Armstrong, Oak Ridge National Laboratory, and T. Dubois, U.S. Army CECOM.

K. Scott Weil, John E. Deibler, John S. Hardy, L. A. Chick, and **Chris A. Coyle,** Energy Science and Technology Division, Pacific Northwest National Laboratory, Richland, WA 99352; **Dong Sang Kim** and **Guan-Guang Xia,** Environmental Technology Division, Pacific Northwest National Laboratory, Richland, WA 99352. Contact e-mail: scott.weil@pnl.gov.

There are essentially two standard methods of sealing, compressive sealing and rigid bonding, each of which has its own set of merits and weaknesses. In compressive sealing, a compliant high-temperature material is captured between the two sealing surfaces and compressed, using a load frame external to the stack, to deliver hermetic sealing in the same way that rubber compression gaskets are used in everyday appliances. Because the seal conforms to both sealing surfaces and is under constant compression during use, it forms a dynamic seal. That is, the sealing surfaces can slide past one another without disrupting the hermeticity of the seal and coefficient of thermal expansion (CTE) matching is not required between the ceramic cell and the metal separator. At present, however, this technology remains incomplete due to the lack of a reliable high-temperature sealing material that would form the basis of the compressive seal. A number of materials have been considered, including mica, nickel, and copper, but each has been found deficient for any number of reasons, ranging from oxidation resistance in the case of the metals to poor hermeticity and through-seal leakage in the case of mica.[2] An additional difficulty is in designing the load frame, as it must be capable of delivering moderate-to-high loads in a high-temperature, oxidizing environment over the entire period of stack operation. Material oxidation and load relaxation due to creep, as well as added expense and additional thermal mass that must be heated, cooled, and maintained at temperature under equilibrium operation are all issues that require particular attention with this type of seal design. Due to these constraints and specifically because our application is an auxiliary power unit (APU) targeted for automobile and truck use where minimization of device weight and volume are critical, our research has focused on the development of rigid seals, such as glass joining.

Historically, glass joining is a cost effective and relatively simple method of bonding ceramic and metal parts. However the softening point of the glass typically limits the maximum operating temperature to which the joint may be exposed. In addition, the final seal is brittle, non-yielding, and particularly susceptible to fracture when exposed to tensile stresses, for

example, the type encountered during non-equilibrium thermal events such as stack heating and cooling. For this reason, in stack designs that use glass seals it is imperative that the temperature-dependent CTEs for each of the joining components, i.e., the ceramic cell, the seal, and the metal separator, are approximately equal to minimize the build up of residual stresses within the joint. Only a handful of high-temperature glass compositions in the borate- or phosphate-doped aluminosilicate families currently satisfy this requirement.[3] Additionally, as listed in Table 1 there are a number of other key materials and processing variables that affect the performance of this type of seal, including the composition of the metal substrate against which the seal is made, as well as operating parameters such as the expected lifetime of the device (and therefore the seals), and the degree of thermal cycling to which the seals will be exposed during system operation. For a generic APU application, target values for these performance figures are 5000-10 000 h at a nominal operating temperature of 750 °C and 5000 rapid thermal cycles (≥75 °C/min during stack heating and ≥10 °C/min upon cooling), respectively.[4]

The effects of these variables on joint strength can be investigated using traditional methods of mechanical analysis such as tensile and torsion testing. If conducted carefully, these tests provide a highly accurate, quantitative measure of joint strength. However, in practice, these techniques are not especially conducive to a development program where rapid specimen fabrication, testing, seal modification, re-testing, etc., are essential to success. Specifically, test specimen preparation and alignment of the specimen in the test fixture can be particularly difficult and laborious. An alternative method of testing was sought that would allow a much faster turn-around time and facilitate the screening of a large number of materials, processing, and performance parameters. As such, a modified version of a standard rupture testing technique was used as the primary qualification tool in the screen testing effort. The test is conducted by placing a sealed disk specimen in the test fixture and pressurizing the backside of the sample until seal rupture occurs. That is, the specimen is subjected to an accelerated stress test, using air pressure to generate high levels of stress within the seal. The details of the test apparatus and procedure are outlined below along with results that have particular significance to the stack design. In addition, results from metallographic, chemical, and thermal analyses of the test specimens are presented and used to help interpret the rupture strength data.[1]

[1]With the exception of rupture stress, all of our data are reported in conventional SI units. The rupture data is reported in the units that were recorded, i.e., psi. The conversion of measured rupture stress to seal strength (in MPa) is discussed in the results, Section 3.3.

Table 1 Materials, Processing, and Performance Variables Involved in pSOFC Glass Seal Development

Material Variables	Processing Variables	Performance Variables
Glass composition	Binder burn-out conditions	Thermal exposure
Ratio of BaO, Al_2O_3, and SiO_2	Burn-out temperature	Temperature
Minor alloying agents: L_2O_3, CeO_2, and CaO	Hold time at temperature	Time at temperature
Second Phase Additions	Joining temperature	Ambient gas atmosphere
Metal Substrate Effects	Temperature uniformity during sealing	Thermal shock
Scale composition: Cr_2O_3 vs. Al_2O_3	Glass viscosity as a function of soak temperature	Magnitude of ΔT/cm across the seal due to rapid heating/cooling
CTE effects	Time at joining temperature	Thermal cycling
Use of minor alloying agents: Mn, Ti, etc.	Glass viscosity as a function of soak time	Rate of heating/cooling
Ceramic Substrate Effects	Uniformity and magnitude of joining pressure	Number of thermal cycles
YSZ composition: 3, 5, and 8% Y_2O_3 additions	Glass viscosity as a function of sealing pressure	
CTE effects: anode composition	Rate of heating during joining	
Use of substrate surface modifiers		
Coatings		
Surface geometry		

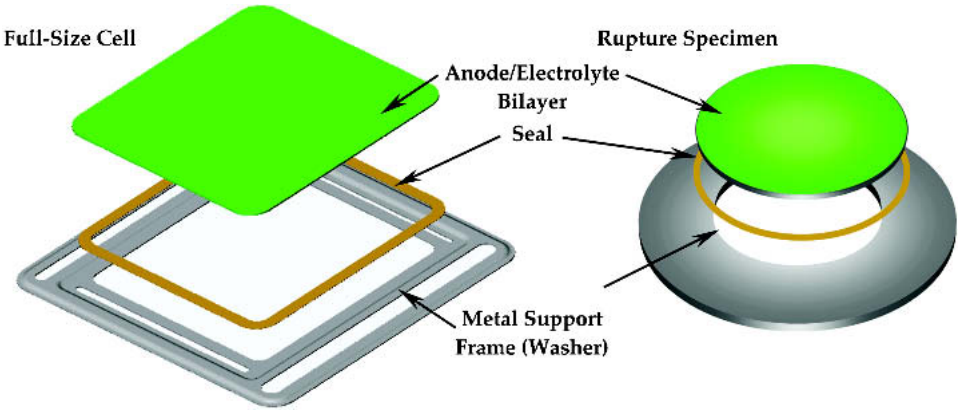

Fig. 1 Comparison of the the full-size SOFC window frame component to the rupture test specimen (not shown to comparative scale).

2. Experimental

2.1 Materials

As shown in Fig. 1, the test employs essentially a miniaturized version of the main fuel cell component as the test specimen. A 25 mm diameter ceramic bilayer is glass sealed directly to a metal washer, of the same composition as the frame used in the pSOFC stack, that measures 44 mm in outside diameter with a 15 mm diameter concentric hole. Like the actual ceramic pSOFC cell, the anode-supported bilayer coupons consist of NiO-5YSZ as the anode and 5YSZ as the electrolyte. The bilayer coupons were fabricated by tape casting and cosintering techniques developed at Pacific Northwest National Laboratory.[5] To prepare the anode layer, NiO (J.T. Baker, Inc., Phillipsburg, NJ), 5YSZ (Zirconia Sales, Inc.), and carbon black (Columbia) powders were ball milled together in a 38:25:37 volume percent ratio for 1½ days with a proprietary binder and dispersant system in a 2-butanone/ethyl alcohol solvent. The slurry was cast onto silicone-coated mylar, forming a ~0.4 mm thick tape after solvent evaporation. The electrolyte tapes were prepared by ball milling 5YSZ with a proprietary binder and dispersant system in 2-butanone/ethyl alcohol for 2 days and casting the slurry by the doctor blade technique onto silicone-coated mylar to form tapes with an as-dry thickness of approximately 50 μm. The anode and electrolyte tapes were then laser cut into 100 × 100 mm plies. Multiple plies of the anode tape were laminated together with a single ply of the electrolyte tape through a combination of heat and pressure to form a single green bi-layer tape. Disks measuring 30 mm in diameter were cut from the laminated tape using a circular hot knife. The green parts were then sintered in air at 1350 °C for 1 h, yielding finished bi-layer components that measured nominally 25 mm in diameter by 600 μm in thickness, with an average electrolyte thickness of ~8 μm.

Listed in Table 2 are eight different compositions of ferritic stainless steel that were selected for testing, five of which form a protective chromia scale upon high temperature air exposure (Al 29-4, Crofer-22 APU, E-Brite 26-1, 430, and 446) and three that form an alumina scale (Alpha-4, Fecralloy, and aluminized 430). Ferritic stainless steels are under strong consideration for use in SOFCs and other solid state electrochemical devices because: (a) they form protective oxide scales, giving them excellent oxidation resistance properties at the use temperature of 700-800 °C, (b) their CTEs closely matches that of the NiO-YSZ/YSZ bilayer, and (c) they can be readily produced as sheet products in large quantitiy at low cost. With the exception of Durafoil, each steel was a procured as 300 μm thick sheet in the as-annealed condition. The Durafoil was obtained as 50 μm thick sheet. The flat washer-shaped specimens were cut from the sheets via electrical discharge machining and edge burrs were removed by lightly grinding. The samples were then flushed with deionized water ultrasonically cleaned in acetone for 10 min, and wiped with methanol prior to use.

The glass seal composition used in this study, designated as G-18, was an in-house designed barium calcium aluminosilicate based glass originally melted from the following mixture of oxides (by weight percent): 56.4% BaO, 22.1% SiO_2, 5.4% Al_2O_3, 8.8% CaO, and 7.3% B_2O_3.[6] The G-18 powder was milled to an average particle size of ~20 μm and mixed with a proprietary binder system to form a paste that could be dispensed onto the substrate surfaces at a uniform rate of 0.075 g/linear-cm using an automated syringe dispenser. In this manner, the glass paste was dispensed onto the YSZ side of the bilayer discs. Each disk was then concentrically positioned on a washer specimen, loaded with a 100 g weight, and heated in air under the following sealing schedule: heat from room temperature to 850 °C at 10 °C/min, hold at 850 °C for 1 h, cool to 750 °C at 5 °C/min, hold at 750 °C for 4 h, and cool to room temperature at 5 °C/min.

2.2 Testing

Potentially there are several ways in which a rigid glass pSOFC seal can fail during operation, including the following:

- *Failure by fracture under pressurization.* The glass seal can be viewed essentially as a multicomponent laminate composite composed of (at a minimum): the electrolyte membrane (i.e., the YSZ), the sealing glass, and the oxide scale that naturally forms on the metal substrate during stack sealing and operation. Each of these layers is a brittle material and as such, each is susceptible to failure by brittle fracture. Although under operation the pressure differential across the positive electrode, electrolyte, negative electrode (PEN) membrane in an actual full-scale pSOFC stack is relatively small, typically 2-6 psi (13.8-41.4 kPa),

Table 2 Ferritic Stainless Steel Composition

	Nominal Composition, wt.%											
Alloy	**Ni**	**Cr**	**Fe**	**Mo**	**C**	**Mn**	**Si**	**Al**	**P**	**S**	**N**	**Others**
Al 29-4	0.15	29.0	Balance	4.0	0.01	0.3	0.2	…	0.025	0.02	0.015	…
Alpha-4 (Durafoil)	…	21.0	Balance	…	…	…	…	6.3	0.02	0.02		0.1 Ce + La
Crofer-22 APU	…	22.8	Balance	…	0.005	0.45	…	…	0.016	0.002	0.01	0.08 Ti + 0.06 La
E-Brite 26-1	0.09	26.0	Balance	1.0	0.001	0.01	0.025	…	0.02	0.02	0.01	0.03 Cu
Fecralloy	…	22.0	Balance	…	0.03	…	…	5.3	0.02	0.02	0.01	0.10 Y + 0.01 Zr
430	…	17.0	Balance	…	0.12	1.0	1.0	…	0.04	0.03	0.25	…
Aluminized 430	…	17.0	Balance	…	0.12	1.0	1.0	5.0	0.04	0.03	0.25	…
446	…	25.0	Balance	…	0.020	1.50	1.00	…	0.04	0.03	0.25	…

the stress within the seal is magnified by over five times due to the difference in load carrying area between the PEN and the peripheral seal. Thus, if a large-enough flaw exists in any of the materials within the seal or if residual tensile stresses of a minimum critical value develop due to thermal expansion mismatch between components or warping due to non-uniform heating within a given component, fracture can occur.[7]

- *Failure during rapid thermal cycling*. Transient thermal events can occur by accident (e.g., due to a loss of fuel) or by design, such as the need for rapid system start-up as is required in a transportation APU application. Thermal gradients arising during rapid heating or cooling can generate out-of-plane bending stresses that may lead to failure in one of the brittle components in the ceramic-to-metal joint. In addition, thermal cycling may lead to fatigue problems in both the metal and ceramic components. Specifically in ceramics materials, this can occur due to the cyclic growth of a sub-critical internal flaw to a critical size under even small thermally generated stresses.[8]
- *Failure upon thermal aging*. The barium aluminosilicate glasses used in pSOFC sealing typically display signs of devitrification within the first few hours of exposure at operating temperature.[3,9] As the glass begins to crystallize, its carefully engineered thermal expansion properties will change and continue to evolve with time at operating temperature, which can ultimately limit the number of thermal cycles and the rate of cycling at which the joints are capable of surviving.[10] In addition, compositional and microstructural changes induced by long-term thermal diffusion are likely to take place at the seal/substrate interfaces, which may also lead to seal degradation and subsequent failure.

With the above modes of failure in mind, our objective was to screen potential pSOFC joining systems, i.e., metal substrates and sealing materials, under sequentially more aggressive conditions in an effort to identify the most promising sealing candidates. In this way, seals were first rupture tested in the as-joined condition. Joining systems that were considered viable were then re-tested after prolonged thermal exposure and/or upon multiple heating and cooling cycles. Aging tests were conducted by exposing the sealed test specimens to ambient air at 750 °C for a given period of time. Thermal cycle testing was performed by heating the specimens in air to 750 °C in 10 min using an infrared furnace, holding at temperature for 10 min, and cooling to ≤70 °C in 40 min before reheating under the same conditions for a given number of cycles.

A schematic of the experimental set-up used in rupture testing is illustrated in Fig. 2(a), and a photo of the device is shown in Fig. 2(b). The test sample was placed within a fixture that consists of a bottom and top flange, a coupling that secures and centers the two flanges, and an O-ring that is squeezed against the bottom surface of the washer. We found that the dimensions of the two flanges and the O-ring relative to those of the specimen and the amount of torsion used to compress the O-ring can play a role in defining the rupture stress of the sealing specimen. Thus, these parameters were held fixed at the values listed in Table 3 so that batch-to-batch comparisons could be made. Compressed air was used to pressurize the backside of the washer specimen up to a maximum rated pressure of 150 psi (1.03 MPa). A digital regulator allows the pressure behind the joined bilayer disk to be slowly increased to a given set point. This volume of compressed gas can be isolated between the specimen and a valve, making it possible to identify a leak in the seal by decay in pressure. In this way, the device can be used to measure the hermeticity of a given seal configuration without causing destructive failure of the seal. Alternatively, by increasing the pressure to the point of specimen rupture, the maximum pressure that the specimen can withstand can be measured. A minimum of six specimens was tested for each joining condition.

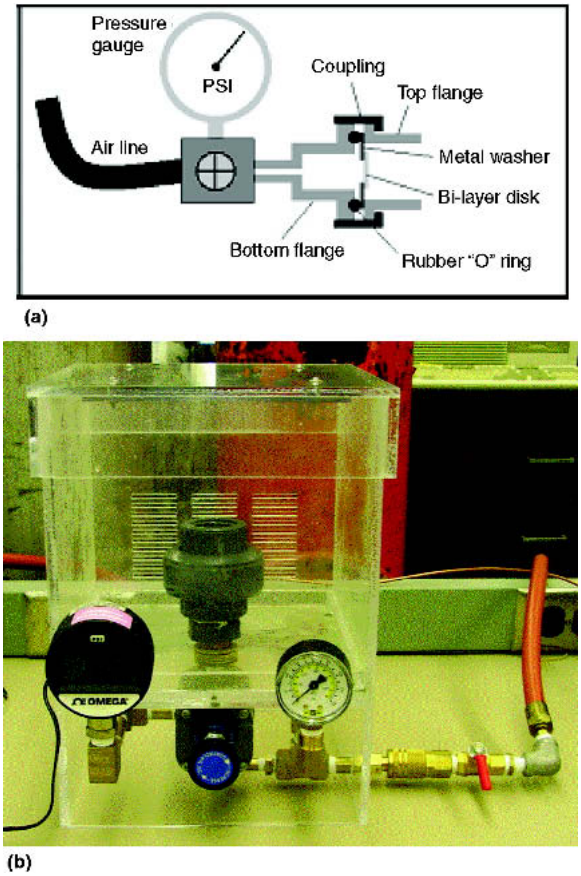

Fig. 2 **(a)** Schematic illustration of the rupture test apparatus; **(b)** photo of the test aparatus and specimens

Table 3 Specimen and Fixture Dimensions

Component	Dimensions		
Anode/electrolyte bilayer disk	25 mm O.D.		600 μm thick
Metal substrate	44 mm O.D.	15 mm I.D.	300 μm thick
Viton O-ring	35 mm O.D.	29 mm I.D.	
Top Flange	46 mm O.D.	29 mm I.D.	
Bottom Flange	46 mm O.D.	24 mm I.D.	
Compression		15 in-lbs torsion	

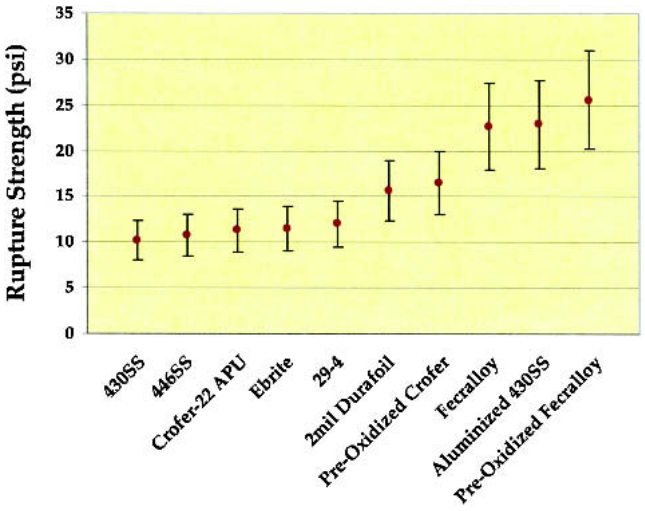

Fig. 3 Rupture strength of as-joined PEN/glass/interconnect specimens as a function of metal substrate composition

It is important to recognize that as stated above, the differential pressure that will arise across each individual PEN in an actual operating stack is actually quite small. That is, the rupture strength test places the PEN, seal, and metal interconnect material under a highly exaggerated stress condition relative to prototypic steady-state operation (but as will be discussed, the test appears to approximate transient-state operation, specifically rapid stack heating). In this way, the test allows identification of the weak link in the sealing system, i.e., the ceramic substrate, the sealing glass, the metal substrate and associated oxide scale, or any of the interfaces in between, so that the seal can potentially be improved in the next round of development. Ideally for the purposes of quantitative comparison one would like the stress in the seal to be either pure shear or pure tension at failure. Unfortunately, the stress state in the rupture test specimen is mixed-mode. However, as will be discussed, the range of rupture pressures at failure for a given batch of specimens fabricated and tested under identical conditions was, in general, fairly small and the average rupture pressure for the batch provided a useful figure of merit that could be used to compare with other batches joined or tested under a different set of conditions.

In a number of cases after rupture testing, further analysis was carried out to determine why failure took place and how joining and sealing could potentially be improved. Microstructural analysis of the joints after rupture testing was conducted on polished cross-sectioned samples using a JEOL JSM-5900LV scanning electron microscope (SEM; JEOL Corp., Peabody, MA) equipped with an Oxford energy dispersive x-ray analysis (EDX) system that employs a windowless detector. To avoid electrical charging of the samples, they were carbon coated and grounded prior to analysis. Elemental profiles were determined across the joint interfaces in the line-scan mode. Measurements of CTE as a function of temperature were conducted on 25 × 3 × 3 mm bars of bulk glass and 25 mm long × 3 mm diameter rolled metal foil samples in the as-formed and as-aged conditions using a Unitherm model 1161 dilatometer (Anter Corp., Pittsburgh, PA). Room temperature x-ray diffraction (XRD) analysis of the nascent and aged G-18 was performed on powder samples using a Philips Wide-Range Vertical Goniometer and a Philips XRG3100 x-ray Generator (Philips Corp., Eindhoven, The Netherlands) over a scan range of 20-80° 2θ with a 0.04° step size and 1 s hold time. XRD pattern analysis was conducted using Jade 6+ (EasyQuant, New York, NY) software. All XRD specimens were prepared using the same specimen holder and preparation technique to ensure sample consistency.

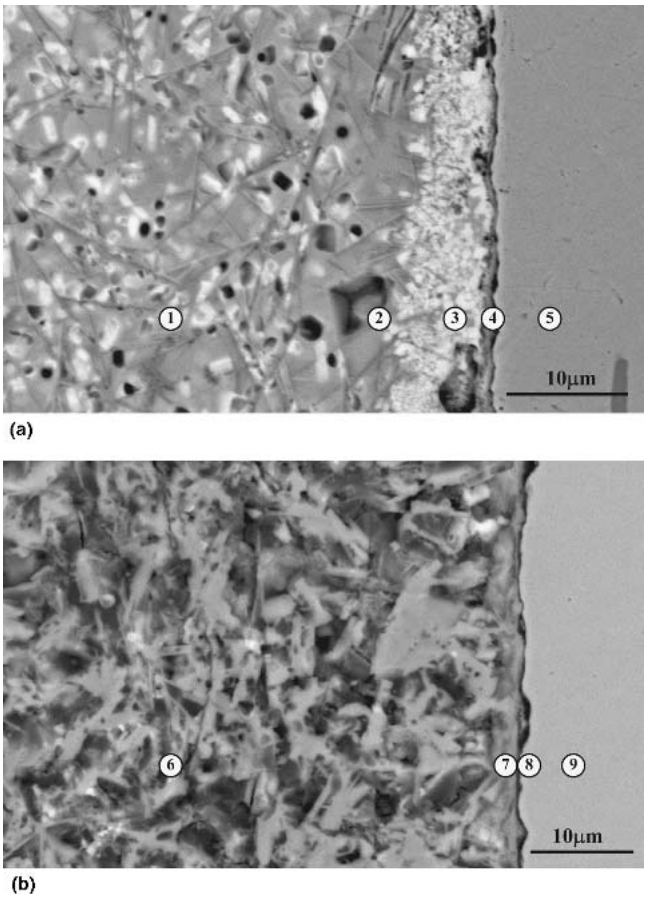

Fig. 4 **(a)** Glass/metal interface against a representative chromia former, 446; **(b)** glass/metal interface against a representative alumina former, fecralloy

Table 4 Local EDS Results for Points Marked in Figures 3(a) and (b)

	Composition, at.%						
Element	**O**	**Al**	**Si**	**Ca**	**Cr**	**Fe**	**Ba**
Point 1	57.4	3.8	18.2	2.6	…	…	18.0
Point 2	55.9	19.2	19.6	1.9	…	…	3.4
Point 3	65.1	1.9	4.2	0.6	13.3	0.2	14.7
Point 4	57.8	0.8	1.9	1.0	35.9	0.6	2.0
Point 5	…	…	…	…	23.3	76.3	…
Point 6	55.9	5.4	19.6	1.3	…	…	17.8
Point 7	59.0	14.8	16.3	1.3	1.7	0.3	6.6
Point 8	52.9	36.8	0.1	…	6.7	3.5	…
Point 9	…	4.3	0.5	…	21.6	73.6	…

3. Results and Discussion

3.1 Effects of Interconnect Composition on Rupture Strength

Plotted in Fig. 3 is rupture strength as a function of interconnect composition. The results show that rupture strength is measurably higher when an alumina-forming alloy is used in the seal instead of a chromia-former. Microstructural analysis suggests that the root cause for this difference in joint strength lies at the interface between the bulk glass and the metal substrate. Shown in Fig. 4(a) and (b) are the representative cross-sectional micrographs of the glass/metal interface for a chromia-former, 446 stainless steel, and an alumina-former, FeCrAlY. Corresponding chemical analysis of each of the regions labeled in the two figures via EDX are listed in Table 4.

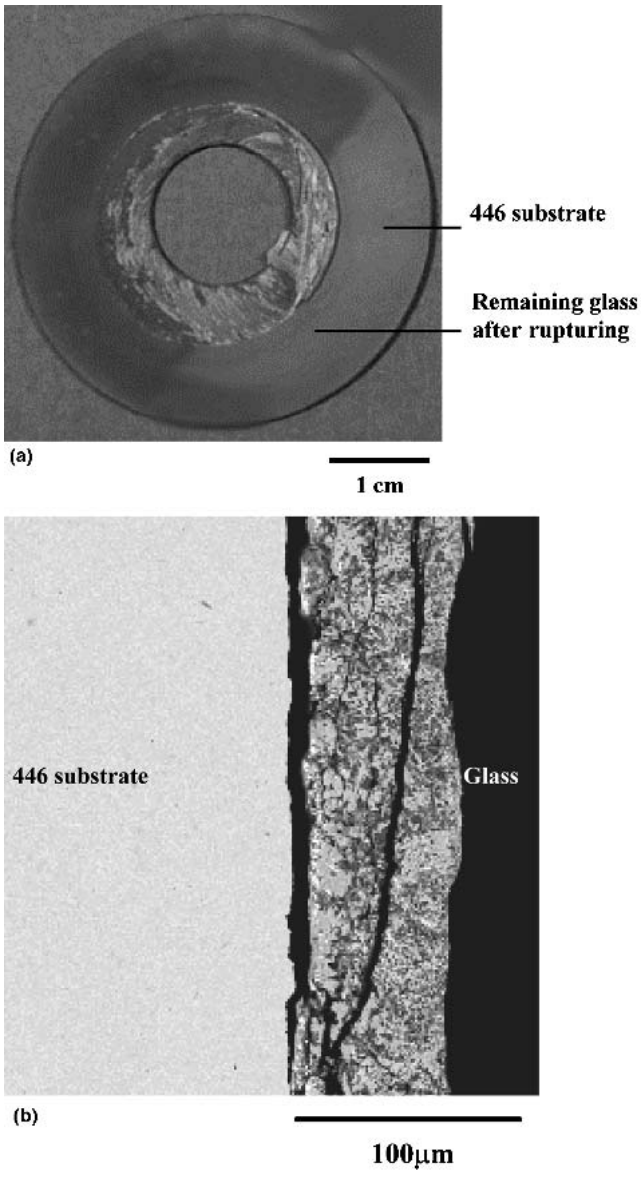

Fig. 5 **(a)** Planar view of a ruptured G-18/446 specimen; **(b)** cross-sectional view of the ufractured portion of the same specimen; note the complete delamination within the interfacial region between the glass and the metal substrate

It is apparent from both figures that the glass seal material devitrifies to a considerable extent in the short time period over which joining takes place, forming several crystalline phases in the remaining glassy matrix, notably: $BaSiO_3$ (oblate white crystals), $BaAl_2Si_2O_8$ (needle-shaped dark gray crystals), and $Ba_3CaSi_2O_8$ (large, blocky gray crystals), with the matrix composed of 13 mol% Si, 9.6 mol% Ba, 6.1 mol% Ca, 2.9 mol% Al, and 67.1 mol% O. Five microstructurally distinct zones can be readily observed in the micrograph of the G-18/446 joint shown in Fig. 4(a): (1) the devitrified glass-ceramic in the bulk portion of the seal, (2) an adjacent glass-ceramic region that is measurably depleted in barium, (3) a ~10 μm thick reaction zone between the chromia scale and the glass, (4) a chromia scale that forms on the surface of the alloy during joining, and (5) the bulk 446 stainless steel. EDX analysis conducted on Region (3) indicates that the primary phase in the interfacial reaction zone is $BaCrO_4$. From oxidation studies conducted on 446, the parabolic rate constant associated with chromia growth on the alloy is 3.43×10^{-14} cm^2/s at 850 °C.[11] Using Wagner's equation[12] for the rate of protective scale growth, one can estimate the maximum thickness of chromia expected to form on the 446 during joining, $t_{1h,850°C} \sim 0.1$ μm. Apparently the chromia scale reacts directly with baria in the glass to form the chromate product. This is consistent with the depletion of barium and lack of chromium observed in the material of Region (2).

Barium chromate was also found on the exposed surface of the bulk glass, causing a yellow coloration on the normally white devitrified material. Yang et al.[13] have examined the reactions that lead to the formation of $BaCrO_4$ due to reaction between chromia and G-18 glass. They found that the interfacial product observed in Fig. 4(a) results primarily from the following two reactions:

$$2Cr_2O_3(s) + 4BaO(s) + 3O_2(g) \rightarrow 4BaCrO_4(s) \quad \text{(Eq 1)}$$

$$CrO_2(OH)_2(g) + BaO(s) \rightarrow BaCrO_4(s) + H_2O(g) \quad \text{(Eq 2)}$$

where in the second reaction, chromium oxyhydroxide $[CrO_2(OH)_2]$ forms due to a reaction at moderate temperature between the chromia scale and water in the binder or

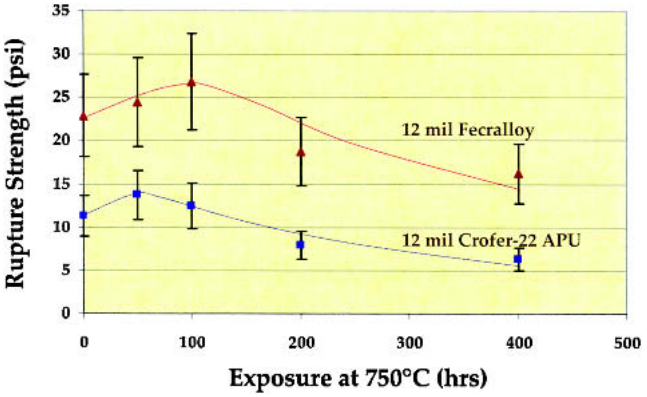

Fig. 6 Rupture strength of bilayer/glass/fecralloy and bilayer/glass/Crofer-22 APU specimens as a function of exposure time in 750 °C ambient air

ambient air. Thus, both reactions require open access to the chromia/G-18 interface to ambient air at moderate to high temperature for some period of time during the joining process. We believe this is possible during the initial heating step, just after the organic binder of the paste burns out and forms a network of interconnected porosity but prior to densification of the sealing material due to solid state sintering and viscous flow at the joining temperature. Barium chromate has an orthorhombic crystal structure and possesses the following coefficients of thermal expansion over a temperature range of 20-813 °C: $\alpha_a = 16.5 \times 10^{-6}$ K^{-1}, $\alpha_b = 33.8 \times 10^{-6}$ K^{-1}, and $\alpha_a = 20.4 \times 10^{-6}$ K^{-1}.[14] Measurements of the bulk G-18 sealing glass and the 446 alloy over the same temperature range reveal corresponding average CTEs of 11.8×10^{-6} K^{-1} and 12.6×10^{-6} K^{-1}, respectively. The significant difference in CTE between the barium chromate reaction zone and the metal substrate and the bulk glass leads us to believe that cracking and/or delamination in these regions of the seal are likely to occur due to the development of elastic thermal mismatch stresses.

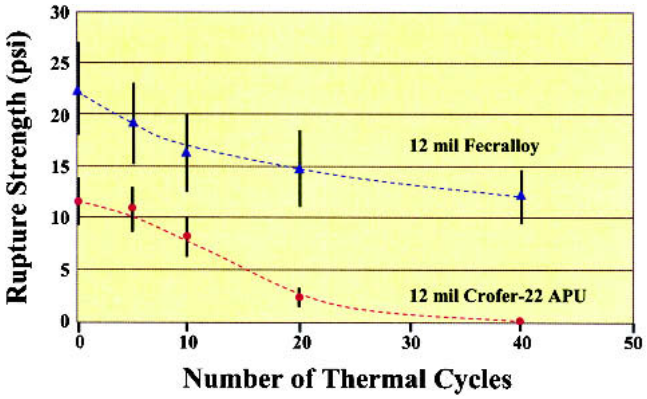

Fig. 7 Rupture strength of bilayer/glass/fecralloy and bilayer/glass/Crofer-22 APU specimens as a function of the number thermal cycles between room temperature and 750 °C

In contrast, the FeCrAlY forms a much thinner oxide scale during sealing, in this case composed primarily of alumina, and subsequently exhibits a much thinner reaction zone between the bulk glass and the scale. At 5.13×10^{-16} cm^2/s,[15] the oxidation rate of FeCrAlY at 850 °C is almost two orders of magnitude lower than that of 446. Thus, when exposed to 850 °C air during the sealing step, the alloy will develop a scale that is less than 0.01 μm thick. From the EDX analysis, the composition of the interfacial reaction zone corresponds to celsian, or $BaAl_2Si_2O_8$. This compound commonly assumes one of two crystal structures during formation, either a hexagonal crystal structure, referred to as hexacelsian with an average CTE of 8.2×10^{-6} K^{-1}, and a monoclinic structure, called monocelsian with an average CTE of 2.7×10^{-6} K^{-1}.[16] Although monocelsian is thermodynamically the more stable phase, hexacelsian typically forms preferentially due to more favorable reaction kinetics.[17] We assume this is the case here, at least in the as-joined condition. Thus in cross section, the joining sample in Fig. 4(b) consists of four microstructurally distinct regions: (1) the bulk alloy, (2) a very thin alumina scale, (3) a ~1 μm thick celsian reaction zone, and (4) the bulk devitrified glass. Because the CTE of the hexacelsian is relatively close to that of the stainless steel and the reaction zone is quite thin, thermal expansion mismatch is not as problematic

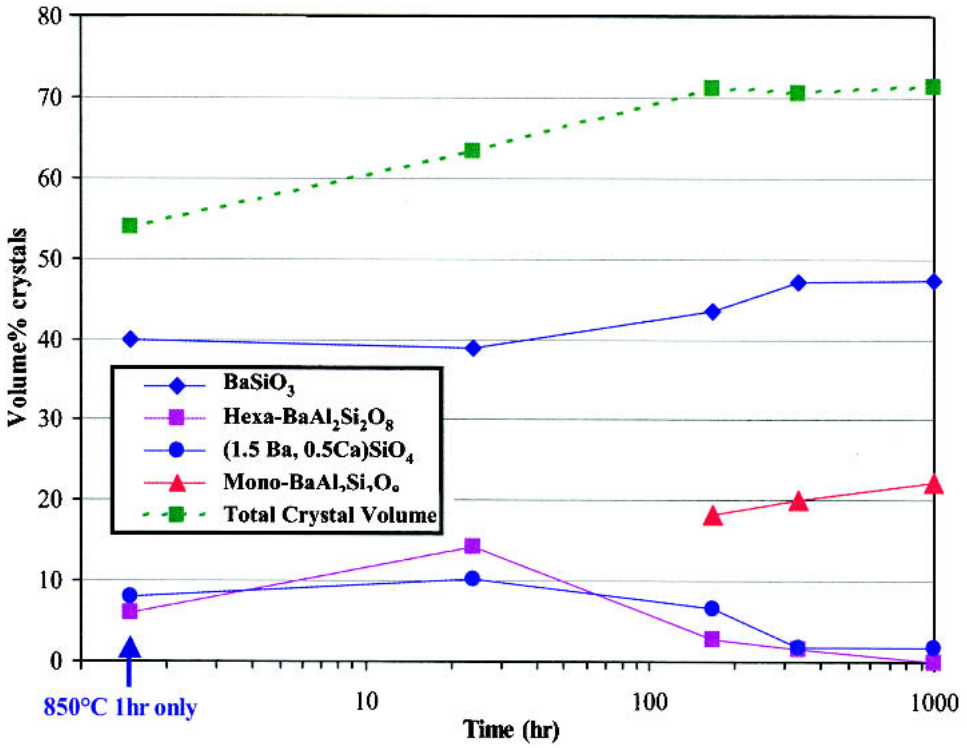

Fig. 8 Quantity of crystalline phase formed in G-18 as a function of time held in air at 750 °C

as in the case of $BaCrO_4$ formation and the resulting joint is stronger.

Post-test failure analysis of the rupture specimens confirms the source of fracture. Shown in Fig. 5(a) and 5(b) are examples of the fracture surface in a G-18/446 sample in planar and cross-section view. In this specimen fracture takes place within the chromate reaction layer. The yellow barium chromate is apparent on both surfaces of the failed sample in Fig. 5(a). Figure 5(b) clearly shows fracture directly through the reaction zone layer. Because $BaCrO_4$ exhibits a higher CTE than either the adjoining metal or glass-ceramic, this interlayer will experience a tensile stress state as the sample is cooled from the joining temperature.

3.2 Effects of Thermal Cycling and Thermal Aging on Rupture Strength

Shown in Fig. 6 and 7 are rupture strength results for seals formed against Crofer-22 and FeCrAlY as a function of exposure time in 750 °C air and as a function of the number of rapid thermal cycles from ≤70 to 750 °C. Note that both operating conditions lead to degradation in seal strength. In the case of thermal aging, there are two reasons for this. As mentioned above, the glass-ceramic microstructure in the bulk of the seal evolves with time at temperature. Presented in Fig. 8 is a plot of crystalline phases that form within the devitrifying glass as a function of time held at 750 °C. This graph was constructed from a series of quantitative XRD measurements conducted on the aged glass-ceramic samples. Note for example that just after sealing at 850 °C the glass has devitrified by ~50% on a volumetric basis. As mentioned in the previous section, the dominant crystalline phases are barium silicate ($BaSiO_3$), barium calcium orthoslicate ($Ba_3CaSi_2O_8$), and hexacelsian ($BaAl_2Si_2O_8$). Under isothermal heating, the glass continues to crystallize up to an aging period of ~120 h, at which point the crystalline make-up of the glass-ceramic levels off at ~70 vol%. Throughout aging, barium silicate remains the primary crystalline component. In fact, the relative amount of this phase slowly increases with time held at temperature. At ~60 h, the metastable hexacelsian constituent begins to transform to the more stable monoclinic structure. We believe it is the formation of this phase that triggers the significant decrease in CTE observed in thermally aged barium aluminosilicate-based glass-ceramics.

Listed in Table 5 are measurements of the average CTEs of the primary crystalline phases in devitrified G-18. Monocelsian by far exhibits the lowest CTE of the group. The net effect is a reduction in the CTE of the glass-ceramic with continuous high temperature exposure, as illustrated in Fig. 9. Upon joining at 850 °C, the CTE of the bulk glass-ceramic nearly matches that of the reduced bi-layer substrate. However after one week of exposure, enough monocelsian has formed to drop the composite CTE by 15%. The CTE increases slightly after

Table 5 Coefficient of Thermal Expansion for Crystalline Phases in Devitrified G-18

Name	Composition	CTE (a)	Temperature Range (°C)
Wollatonite	$CaSiO_3$	9.4	20-200
Calcium orthosilicate	Ca_2SiO_4	10.8-14.4	20-600
Barium calcium orthosilicate	$Ba_3CaSi_2O_8$	12.2-13.8	20-850
Barium Silicates	$BaSi_2O_5$	14.1	20-1000
	$Ba_2Si_3O_8$	12.6	20-1000
	$BaSiO_3$	12.5	20-550
	$BaSiO_3$	9.4	20-1000
Hexacelsian	$BaAl_2Si_2O_8$	8.0	20-1000
Monocelsian	$BaAl_2Si_2O_8$	2.7	20-1000

(a) CTE measured in-house

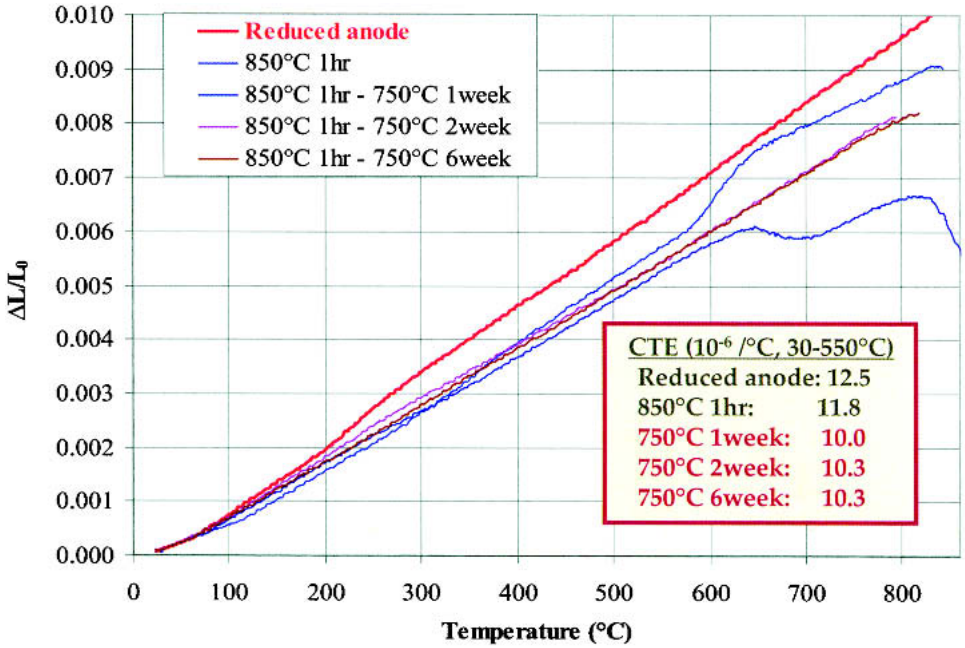

Fig. 9 Thermal expansion of G-18 as a function of temperature after thermally aging in air at 750 °C. Note the expansion curve for the reduced anode (the primary component in the PEN) is included for comparison.

two weeks of exposure with additional formation of $BaSiO_3$, and then stabilizes as the rate of devitrification slows to nearly zero. The reduction in the CTE of the bulk sealing material leads to the development of residual stresses at the glass/metal interface, which can weaken the strength of the seal upon thermal cycling as observed in both our age testing and thermal cycle testing results.

The glass/metal interface also evolves during high-temperature exposure. Cross-sectional SEM examination of the glass/metal interfaces in the aged rupture specimens demonstrated that regardless of the composition of the stainless steel substrate, the reaction zone that develops between the metal's oxide scale and the bulk glass-ceramic thickens with time at temperature. For example in Crofer-22 APU specimens, the barium chromate interfacial product observed in the joint grows from 10 μm thick in the as-joined condition to 44 μm when held for 100 h at 750 °C and to 76 μm when held for a total of 200 h at temperature. Similarly in fecralloy joints, the $BaAl_2Si_2O_8$ grows in thickness from 0.5 to 2 to 3 μm when compared in the as-joined, 100 h exposure, and 200 h exposure conditions. A number of researchers have noted that increasing the thickness of an intermediary layer between two thermally mismatched co-joined layers will increase the overall residual stress in each.[18-20] We presume a similar effect is responsible for the reduction in joint strength with increasing reaction zone thickness observed here. Although detailed microstructural analysis was not conducted on the thermal cycling specimens, we again speculate that changes in the CTE of the bulk sealing material with exposure time and the continuous growth of the interfacial phase play dominant roles in the degradation of seal strength reported in Fig. 7.

3.3 Finite Element Analysis

Finite element analysis of both the baseline rupture specimen and the middle cell of one of the 30-cell pSOFC stacks in our APU design was conducted to determine and compare the relative stress states in each. The middle cell was chosen because in initial stack modeling, it was predicted to exhibit the maximum level of combined tensile and shear stress in the stack during the most aggressive operating condition in our application, i.e., system start-up. The dimensions, material properties, and operating conditions used in modeling these two seal configurations are listed in Table 6. The ANSYS 8.0 software suite was used in the modeling analysis. For the rupture test, it was assumed that the pressure within the specimen is applied symmetrically from the centerline of the PEN out to the radius of the O-ring seal in the testing device. The top side of the washer is constrained in the vertical direction from the top flange radius to the outside edge. Figure 10(a) shows an axisymmetric model of the specimen, where the *y* axis is the axis of symmetry. In this figure each of the components is labeled, with the anode shown as red and the metal washer lighter aqua. Figure 10(b) displays a close up of the seal region which also shows the electrolyte and the applied pressure.

Under this set of conditions, the peak mid-plane seal stress

Table 6 Component Dimensions, Material Properties, and Operating Conditions Assumed in Modeling

	Material Properties		
Dimensions	**Modulus (GPa)**	**Poisson Ratio**	**Operating Conditions**
Rupture Testing			
PEN			Pressurization conducted at room temperature
25 mm O.D., 610 μm thick	…	…	
600 μm thick anode (Ni/5YSZ composite)	105	0.32	
10 μm thick electrolyte (5YSZ)	212	0.31	Specimen pressurized at 10 psi/sec to rupture
Metal Washer			
44 mm O.D., 15 mm I.D., 300 μm thick	…	…	
Ferritic stainless steel	191	0.29 (elastic), 0.5 (plastic)	
Seal			
20 mm O.D., 15 mm I.D., 200 μm thick	…	…	
50% devitrified G-18	74.5	0.3	
Full-Size Stack			
30-cell stack in which each cell is composed of a PEN joined to a metal frame, a separator, and cell-to-cell seals	…	…	Internal heating via 800°C air through the air and fuel manifolds
PENs			
12 × 12 cm, 610 μm thick	…	…	Heating rate: room temperature to 750° C in 10 min, approx. parabolic rate
600 μm thick anode (Ni/5YSZ composite)	$121.3 - 54.6 \times 10^{-3}T$	0.32	
10 μm thick electrolyte (5YSZ)	$228.9 - 54.6 \times 10^{-3}T$	0.31	
Metal Frames			
15 × 15 cm with an 11 × 11 cm centered hole	…	…	Adiabatic external boundary conditions
300 μm thick ferritic stainless steel	$204.8 - 36.1 \times 10^{-3}T$	0.29 (elastic), 0.5 (plastic)	
Metal Separators			
15 × 15 cm	…	…	
300 μm thick ferritic stainless steel	$204.8 - 36.1 \times 10^{-3}T$	0.29 (elastic), 0.5 (plastic)	
Seals			
5 mm wide, 200 μm thick	…	…	
50% devitrified G-18	$77.6 - 44.9 \times 10^{-3}T + 191.8 \times 10^{-6}T^2 - 253 \times 10^{-9}T^3$	0.3	

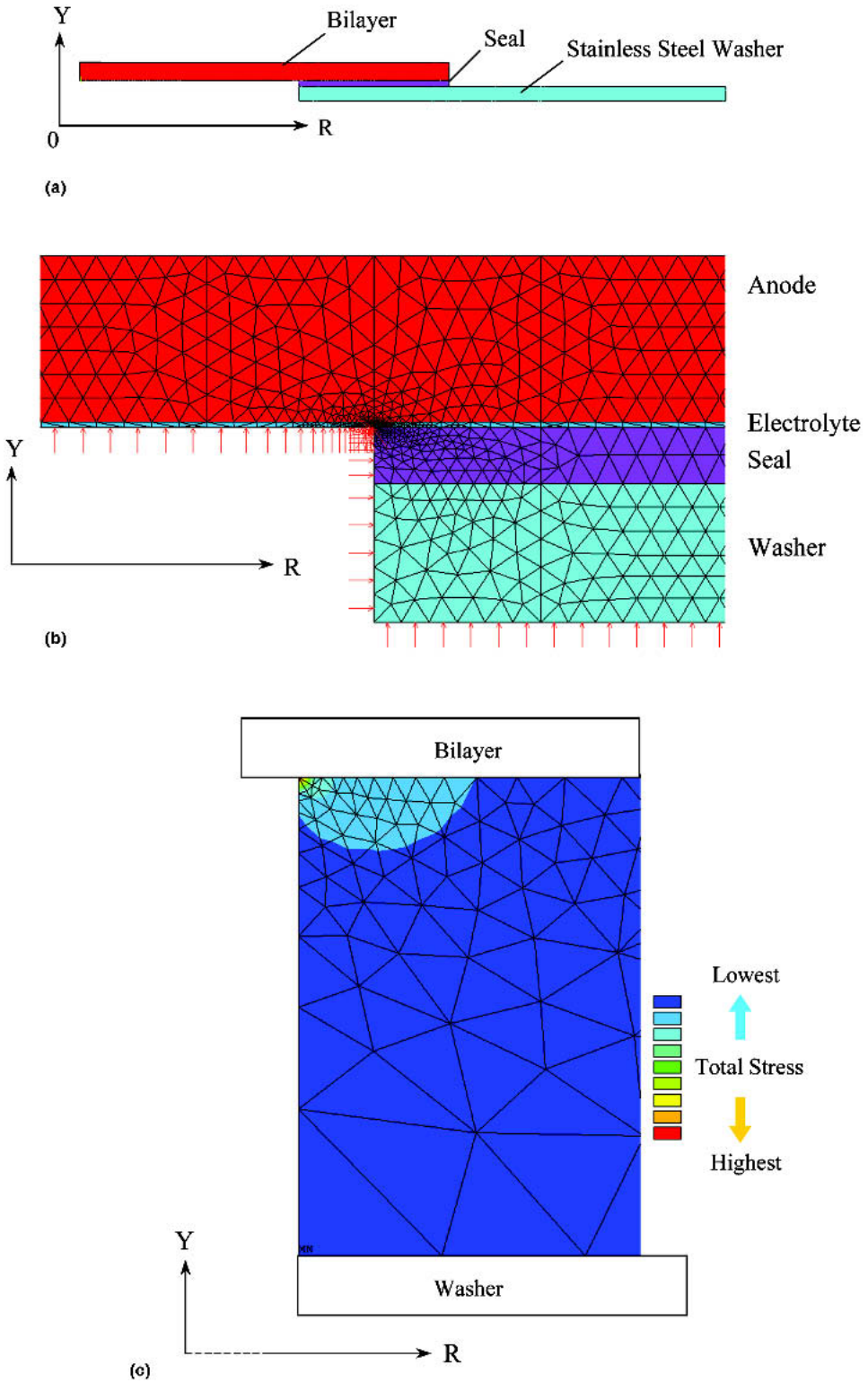

Fig. 10 **(a)** Axisymmetric half-model of the rupture specimen, where the *y* axis is the axis of symmetry; **(b)** finite element mesh for the anode, electrolyte, seal, and metal components in the rupture specimen; **(c)** area of highest stress in the seal is located at the inner corner nearest the electrolyte

is 33.6 times the applied pressure, or translating from psi of applied pressure to SI units (MPa) for seal stress, the conversion factor is 0.231 times the rupture pressure. That is, a rupture pressure of 80 psi equates to a seal stress of 18.5 MPa tension. Figure 10(c) shows that this peak stress is concentrated at the inner corner of the seal in contact with the PEN. Under

the same conditions, the maximum stress within the PEN is 174.8 times the applied pressure, or 1.205 times the applied pressure in terms of the mixed units convention. PEN failure has been observed at rupture pressures of ~130 psi, suggesting that the strength of the PEN is 157 MPa. Independent ball-on-ring biaxial flexure testing (ASTM F 394-78) of the PEN conducted at room temperature yielded an average PEN strength of 187 MPa. That is, within 15-20%, the two measurements agree.

To compare the stress state found in the rupture test specimen to that arising in the middle cell of the full-size stack, the ratio of tensile stress to total stress at the source of highest stress in the seal was used as the figure of merit. In both seal configurations, tensile stress accounts for the largest portion of the total stress and given the brittle nature of the seal, high tensile stresses are likely to be the primary source of brittle failure assuming the material exhibits typical Weibull behavior. It was found that the value of this ratio is 0.63 for the baseline rupture specimen and 0.66 for the middle cell in the stack design when a simulated rapid heating condition is imposed, i.e., heating from room temperature to 750 °C in 10 min using internal air. The near equivalence of these two values suggests that, although the stress states in the two seal configurations are not identical, within the plane of maximum stress the rupture test does approximate the stress condition of the full-size seal under simulated rapid heating.

4. Conclusions

A screening test for glass pSOFC seals has been developed that allows examination of the effects of a wide variety of materials, processing, and operating parameters on the hermeticity and strength of the resulting joint. Through the use of the rupture test, it was determined that alumina-forming ferritic steel substrates offer greater bond strength with the barium aluminosilicate based-glass used here in both the as-joined and exposure tested conditions, i.e., thermal aging and cycling. The dominant factor in joint strength appears to be the composition and thickness of the reaction zone that forms in between the metal's oxide scale and the bulk glass. The barium chromate layer that develops on the chromia-forming steels exhibits poorer thermal expansion matching and tends to grow to a greater thickness than the corresponding celsian zone observed on the alumina-formers.

Acknowledgments

The authors would like to thank Nathan Canfield for his preparation of the ceramic bilayer samples and Nat Saenz, Shelly Carlson, and Jim Coleman for their assistance in the metallographic analysis. This work was supported by the U. S. Department of Energy's National Energy Technology Laboratory (NETL) as part of the Solid-State Energy Conversion Alliance (SECA) Program. The Pacific Northwest National Laboratory (PNNL) is operated by Battelle Memorial Institute for the United States Department of Energy (U.S. DOE) under Contract DE-AC06-76RLO 1830.

References

1. S. Linderoth: "Low-Cost Fabrication and Improved Performance of SOFC Stack Components" in *Proc. Fourth European Solid Oxide Fuel Cell Forum,* European Fuel Cell Forum, Oberrohrdorf, Switzerland, 2000, pp. 19-28.
2. S. P. Simner and J. W. Stevenson: "Compressive Mica Seals for SOFC Applications," *J. Power Sources*, 2001, *102*, pp. 310-16.
3. N. Lahl, L. Singheiser, K. Hilpert, K. Singh, and D. Bahadur: "Aluminosilicate Glass-Ceramics as Sealant in Solid Oxide Fuel Cells" in *Proceedings of the Sixth International Symposium on Solid Oxide Fuel Cells*, The Electrochemical Society, Pennington, NJ, 1999, pp. 1057-65.
4. S. Mukerjee, S. Shafer, J. Zizelman, L. Chick, S. Baskaran, C. Coyle, Y-S Chou, J. Deibler, G. Maupin, K. Meinhardt, D. Paxton, T. Peters, V. Sprenkle, and S. Weil: "Development of a Solid Oxide Fuel Cell Stack by Delphi and Battelle" in *Proceedings of the Ninth International Symposium on Solid Oxide Fuel Cells*, The Electrochemical Society, Pennington, NJ, 2003, in press.
5. S. P. Simner, J.W. Stevenson, K.D. Meinhardt, and N.L. Canfield: "Development of Fabrication Techniques and Electrodes for Solid Oxide Fuel Cells" in *Proceedings of the Seventh International Symposium on Solid Oxide Fuel Cells*, The Electrochemical Society, Pennington, NJ, 2001, pp. 1051-60.
6. K. D. Meinhardt, J. D. Vienna, T. R. Armstrong, and L. R. Pederson, U. S. Patent 6 430 966, 2002.
7. G. Qian, T. Nakamura, and C. C. Berndt: "Effects of Thermal Gradient and Residual Stresses on Thermal Barrier Coating Fracture," *Mech. Mater*., 1998, *27*, pp. 91-110.
8. G. Kirchhoff, M. Holzherr, U. Bast, and U. Rettig: "Thermal Shock and Thermal Cycling Behavior of Silcon Nitride Ceramics," *Key Eng. Mater*., 1994, *89-91*, pp. 605-10.
9. K. Eichler, G. Solow, P. Otschik, and W. Shaffrath: "BAS (BaO-Al_2O_3-SiO_2) Glasses for High Temperature Applications," *J. Eur. Ceram. Soc*., 1999, *19*, pp. 1101-04.
10. N. Lahl, D. Bahadur, K. Singh, L. Singheiser, and K. Hilpert: "Chemical Interactions Between Aluminosilicate Base Sealants and the Components on the Anode Side of Solid Oxide Fuel Cells," *J. Electroch. Soc.*, 2002, *149*, pp. A607-14.
11. Z. Yang, K.S. Weil, D.M. Paxton, and J.W. Stevenson: "Selection and Evalauation of Heat-Resistant Alloys for SOFC Interconnect Applications," *J. Electroch. Soc.*, 2003, *150*, pp. A1188-1201.
12. C. Wagner, *Atom Movements*, American Society of Metals, Cleveland, OH, 1951.
13. Z. Yang, G. Xia, K. D. Meinhardt, K. S. Weil, and J. W. Stevenson: "Chemical Stability of Glass Seal Interfaces in Intermediate Temperature Solid Oxide Fuel Cells" in *Surface, Interfaces, and Science of Joining,* The American Ceramic Society, Westerville, OH (in press).
14. C. W. F. T. Pistorius and M. C. Pistorius, *Z. Kristallogr*., 1962, *117*, pp. 259-63.
15. P. T. Moseley, K. R. Hyde, B. A. Bellamy, and G. Tappin: "The Microstructure of the Scale Formed During the High Temperature Oxidation of a Fecralloy Steel," *Corrosion Sci*., 1984, *24*, pp. 547-65.
16. I. G. Talmy, D. A. Haught, and E. J. Wuchina: "Ceramics in the System $BaO{\bullet}Al_2O_3{\bullet}2SiO_2{\bullet}SrO{\bullet}Al_2O_3{\bullet}2SiO_2$ (BAS-SAS). Polymorphism, Processing, and Properties" in *Proceedings of the 6th International SAMPE Electronics Conference*, SAMPE, Baltimore, MD, 1992, pp. 687-98.
17. D. Bahat: "Kinetic Study on the Hexacelsian-Celsian Phase Transformation," *J. Mater. Sci*., 1970, *5*, pp. 805-10.
18. V. Teixeira, M. Andritschky, W. Fischer, H. P. Buchkremer, and D. Stover: "Effects of Deposition Temperature and Thermal Cycling on Residual Stress State in Zirconia-Based Thermal Barrier Coatings," *Surf. Coat. Technol.*, 1999, *120-121*,pp. 103-11.
19. A. Nordin, and S. Jacobson: "A New Tool for Evaluation of Intrinsic Mechanical Properties of Multilayered Coatings," *Surf. Eng*., 2001, *17*, pp. 465-71.
20. O. Kesler, J. Matejicek, S. Sampath, S. Suresh, T. Gnaeupel-Herold, P. C. Brand, and H. J. Prask: "Measurement of Residual Stress in Plasma-Sprayed Metallic, Ceramic, and Composite Coatings," *Mater. Sci. Eng. A*, 1998, *257*, pp. 215-24.